The shape of the polarization curve and diagnostic criteria

for the metal electrodeposition process control

KONSTANTIN I. POPOV[1,2], PREDRAG M. ŽIVKOVIĆ[1],

BOJAN JOKIĆ[1] and NEBOJŠA D. NIKOLIĆ[2#*]

[1]*Faculty of Technology and Metallurgy, University of Belgrade, Karnegijeva 4, P.O.B. 3503,*

11001 Belgrade and [2]*ICTM-Institute of Electrochemistry, University of Belgrade, Njegoševa 12,*

P.O.B. 473, 11001 Belgrade, Serbia

E-mail: nnikolic@ihtm.bg.ac.rs

Abstract. The simulated shapes of the polarization curves were correlated with the type of metal electrodeposition process control in a function of the exchange current density to the limiting diffusion current density (j_0/j_L) ratios. Diagnostic criteria based on the j_0/j_L ratios were established. For $j_0/j_L > 100$, the system is under the ohmic control. In the range $1 < j_0/j_L \leq 100$ there is the mixed ohmic-diffusion control. The pure diffusion control appears in the range $0.1 < j_0/j_L \leq 1$. For $j_0/j_L \leq 0.1$, the system is activation controlled at the low overpotentials. The proposed diagnostic criteria were verified by comparison of the simulated curves with experimentally recorded ones and by morphological analysis of deposits obtained in the different types of metal electrodeposition process control.
Keywords: lead; zinc; copper; simulation; morphology; scanning electron microscope (SEM).

RUNNING TITLE: Polarization curves and diagnostic criteria

<p style="text-align:center;">INTRODUCTION</p>

Morphology, as the most important characteristic of electrodeposited metal, mainly depends on the kinetic parameters during the electrodeposition process and on the overpotential

---

[#] Serbian Chemical Society active member
*Corresponding author: Dr. N.D. Nikolić; e-mail: nnikolic@ihtm.bg.ac.rs; tel/fax: + 381 11 337 03 89.

30   or current density applied.[1] Also, compositions of electroplating solutions, temperature of

31   electrolysis and the type of working electrode strongly affect the final morphology of

32   electrodeposited metal. The morphology of an electrodeposited metal depends also on the

33   deposition time until the deposit has attained its final form.

34   According to their general kinetic behaviour in aqueous solution, metals can be classified

35   into three classes.[2,3] These classes are:

36   (a) *Class I, so-called normal metals*: Pb, Sn, Tl, Cd, Hg, Ag (simple electrolytes), Zn.

37   These metals have characteristic low melting points and high exchange current densities ($j_0 > 1$ A

38   dm^{-2}; j_0 is the exchange current density). Also, they show high overpotentials for hydrogen

39   discharge.

40   (b) *Class II, intermediate metals*: Cu, Au, Ag (complex electrolytes). These metals are

41   characterised by moderate melting points, medium exchange current densities (j_0 in the interval

42   from 10^{-2} to 1 A dm^{-2}) and lower hydrogen overpotentials.

43   (c) *Class III, inert metals*: Fe, Co, Ni, Mn, Cr, Pt. These metals have high melting points,

44   low exchange current densities and very low hydrogen overpotentials. For this class of metals, j_0

45   is between 10^{-2} and 10^{-12} A dm^{-2}.

46   Formation of the individual and regular grains at lower and dendrites at higher

47   overpotentials is characteristic of electrodeposition processes characterized by extremely large

48   exchange current densities.[1] The spongy deposits are formed at lower overpotentials and

49   dendrites at higher ones during electrodeposition of metals characterized by large exchange

50   current densities. Finally, compact deposits are obtained at lower overpotentials, while both

51   dendritic and spongy-dendritic deposits are formed at higher overpotentials during

52   electrodeposition of metals characterized by medium and low exchange current densities.

53   Obviously, morphology of metal electrodeposits is strictly correlated with the type of

54   control of the electrodeposition process. For example, the activation controlled electrodeposition

55   of copper produces large grains with relatively well defined crystal shapes. This happens at

56   overpotentials belonging to the region of the Tafel linearity.[4,5] At overpotentials situated between

57   the end of the Tafel linearity and the beginning of the limiting diffusion current density plateau

58   (the mixed activation-diffusion control), morphological forms are created by the mass transfer

59   limitations and large grains are not formed.[6,7] Dendrites are formed at overpotentials inside the

60   plateau of the limiting diffusion current density, and at the higher ones at which there is no a

61   hydrogen evolution or hydrogen evolution is not enough to affect hydrodynamic conditions in the

62   near-electrode layer.[8,9] The above consideration is valid for all electrodeposition processes

63   characterized by medium and low values of the exchange current density, in the absence of the

64   noticeable hydrogen evolution reaction.[9] In the presence of strong hydrogen evolution, the

65   honeycomb-like deposits are formed.[9]

66   On the other hand, electrodeposition of metals characterized by the high values of the

67   exchange current density occurs in the conditions of the ohmic, the mixed ohmic-diffusion and

68   only diffusion control of the electrodeposition.[10–12] Formation of spongy deposits at the lower and

69   dendrites at the higher overpotentials was explained by assumption about the diffusion-controlled

70   electrodeposition in the whole range of overpotentials.[10] The linear dependence of the current

71   density on the overpotential is ascribed to the ohmic control,[11] and the regular grains are formed

72   by electrodeposition in this control. In this way, formation of regular particles at lower and

73   dendritic deposits at higher overpotentials in the mixed ohmic-diffusion control can be

74   explained.[12]

75   Simultaneously, the shape of the polarization curves strongly depends on the exchange

76   current density values. The limiting diffusion current density (j_L) values are other important

77   characteristic of electrodeposition systems, indicating on the strong dependence of the shape of

78   polarization curves on the j_0/j_L ratios. Since the continuous change of the exchange current

79   density to the limiting diffusion current density (j_0/j_L) ratios on the shape of the polarization

80   curves can be only obtained by the digital simulation, the software MathLab will be used to

81   examine the dependence of the shape of polarization curve on j_0/j_L ratios. This will enable to

82   establish diagnostic criteria relating the shape of polarization curves through j_0/j_L ratios with the

83   type of electrodeposition control. The proposed diagnostic criteria will be verified by comparison

84   with experimentally recorded polarization curves and by morphologies of deposits obtained in the

85   different types of electrodeposition control.

86

87   EXPERIMENTAL

88

89   Polarization curves for electrodeposition of lead, zinc and copper were recorded from the

90   following solutions:

91   (a) 0.050 M $Pb(NO_3)_2$ in 2.0 M $NaNO_3$,

92   (b) 0.10 M $Pb(NO_3)_2$ in 2.0 M $NaNO_3$,

93   (c) 0.20 M $Pb(NO_3)_2$ in 2.0 M $NaNO_3$,

94   (d) 0.40 M $Pb(NO_3)_2$ in 2.0 M $NaNO_3$,

95   (e) 0.45 M $Pb(NO_3)_2$ in 2.0 M $NaNO_3$,

96   (f) 0.10 M $ZnSO_4$ in 2.0 M $NaOH$,

97   (g) 0.10 M $CuSO_4$ in 0.50 M H_2SO_4.

98

99   Experimental procedure for recording of the Pb polarization curves is given in Refs.[13,14]

100   For the morphological analysis of deposits, lead, copper and zinc were electrodeposited

101   potentiostatically at overpotentials of 10, 50 and 100 mV (Pb), 90, 210, 650 and 1000 mV (Cu)

102   and 45 and 100 mV (Zn). The times of electrodeposition are indicated in Figure caption.

103   Double-distilled water and analytical grade chemicals were used for the preparation of

104   solutions used for the electrodeposition of all metals. All experiments were performed in an open

105   cell at room temperature on vertical cylindrical copper electrodes. The geometric surface area of

106   copper electrodes was 0.25 cm^2. The reference and counter electrodes were of the same metals as

107   deposited ones.The counter-electrodes were metallic foils with 0.80 dm^2 surface area and placed

108   close to the cell walls. The reference electrodes were wires of the corresponding metals whose

109   tips were positioned at a distance of about 0.2 cm from the surface of the working electrodes. The

110   working electrodes were placed in the centre of a cell, in the same location for each experiment.

111   Morphologies of lead, copper and zinc deposits were examined using a scanning electron

112   microscope – TESCAN Digital Microscopy.

113   Digital simulation was realized using the software MathLab.

114

115   RESULTS AND DISCUSSION

116

117   The polarization curve equation taking the concentration dependence of j_0 into account and

118   the linear dependence of j_0 on the C_s/C_0 ratio is given by Eq. (1):[11]

119
$$j = \frac{j_0(f_c - f_a)}{1 + \dfrac{j_0}{j_L}(f_c - f_a)} \qquad (1)$$

120   To enable a digital simulation of the polarization curve equation for the different j_0/j_L ratios,

121   the Eq. (1) can be re-written in the form:

122
$$\frac{j}{j_L} = \frac{\dfrac{j_0}{j_L}\left(f_c - f_a\right)}{1 + \dfrac{j_0}{j_L}\left(f_c - f_a\right)}$$
(2)

123   being valid for all j_0/j_L ratios and overpotentials. Because of this, this form will be used in

124   discussion of the effect of the j_0/j_L ratio on the shape of the polarization curves. Using the current

125   density – overpotential relationship and the procedure for the determination of the ohmic

126   potential drop, the polarization curves for electrodeposition processes can be successfully

127   simulated.[11,15]

128   In Eqs. (1) and (2), j is the current density, C_s and C_0 are the surface and bulk

129   concentrations of depositing ion, and

130    $$f_c = 10^{\frac{\eta}{b_c}} \quad \text{and} \quad f_a = 10^{-\frac{\eta}{b_a}}$$
(3)

131   where b_a and b_c are the cathodic and anodic Tafel slopes and η is the overpotential. The Eqs. (1)

132   and (2) are modified for use in electrodeposition of metals using the values of the cathodic

133   current density and overpotential as positive. In Eqs. (1) and (2), the ohmic potential drop is not

134   included in the overpotential values. Equations (1) and (2) are operative if IR error is eliminated

135   by using the electronic devices that distinguish the superfast change in potential that occurs in

136   this IR portion, when the current density is switched on and off from the slower change of the

137   electrode potential itself, where the charging of the interfacial capacitor takes time.[15] In this way,

138   the polarization curves which do not include the ohmic potential drop can be simulated using Eq.

139   (2).

140   In any other case the measured value of overpotential, η_m, include the ohmic potential drop

141   and it is given by

142    $$\eta_m = \eta + j\frac{L}{\kappa}$$
(4)

143   where L is the length of the electrolyte column between the tip of a liquid capillary and the

144   electrode and κ is the specific conductivity of the electrolyte. Hence, the polarization curves

145   which include ohmic potential drop can be simulated by using the Eqs. (2) and (4).

146

147   *Simulation of polarization curves*

148

149   The polarization curves without included the ohmic potential drop for different j_0/j_L ratio

150   values for both, one and two electron reactions, are shown in Fig.1. They are obtained by using

151   the Eq. (2) for the different j_0/j_L ratios for a different η, b_a and b_c values in the dependence of the

152   mechanism of electrodeposition reactions. From Fig. 1, it is a clear that these dependencies are

153   similar to each others for the large values of the j_0/j_L ratio and at any low value of overpotential.

154   Because of this, the polarization curves without included the ohmic potential drop are not suitable

155   and, for that reason, will not be treated further.

a)

b)

c)
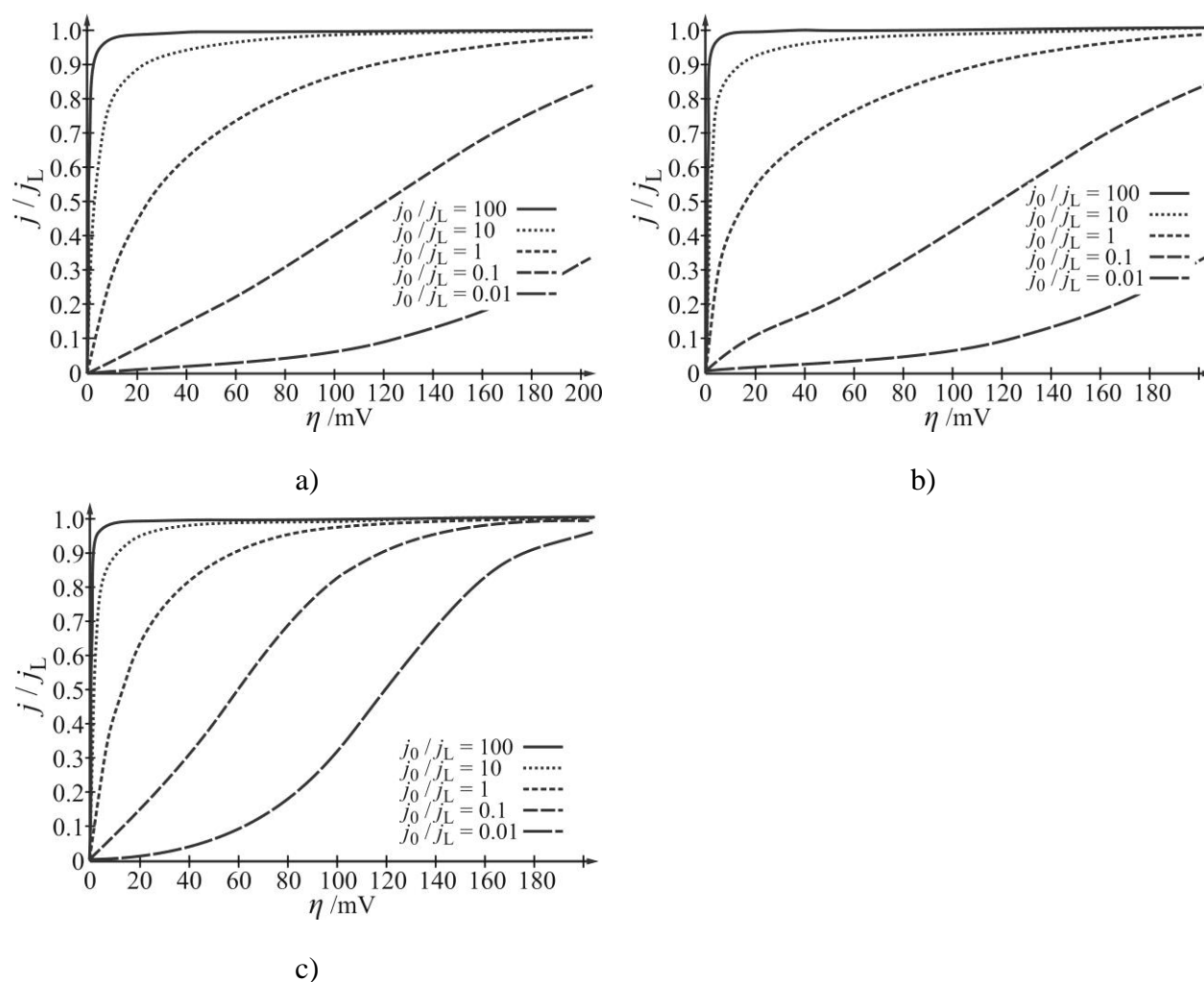
156   Figure 1. Dependencies j/j_L - η calculated using the Eqs. (2) and (3) for the different values of

157   j_0/j_L ratio: a) $b_a = 120$ mV dec^{-1}, $b_c = 120$ mV dec^{-1}, b) $b_a = 40$ mV dec^{-1}, $b_c = 120$ mV

158   dec^{-1} and c) $b_a = 60$ mV dec^{-1}, $b_c = 60$ mV dec^{-1}.

159

160   The simulated polarization curves with included the ohmic potential drop are shown in

161 Fig. 2. They are obtained using the same data as those shown in Fig. 1 and for $j_L = 50$ mA cm^{-2}, L

162 $= 0.2$ cm and $\kappa = 0.1$ S cm^{-1}. In all cases, for $j_0/j_L = 100$ there is linear dependence of the current

163 density on overpotential up to $j = 45$ mA cm^{-2}, or to $j/j_L \approx 0.9$. In these cases, the overpotential

164 without included ohmic potential drop (see Fig. 1) is very low and the measured overpotential is

165 practically equal to the ohmic potential drop between the working and the reference electrodes.

166 Hence, for $j_0/j_L > 100$ there is the ohmic control of the electrodeposition process. It is obvious that

167 the shape of the linear part of polarization curve does not depend on the mechanism of the

168 electrode reaction.

a)

b)

c)
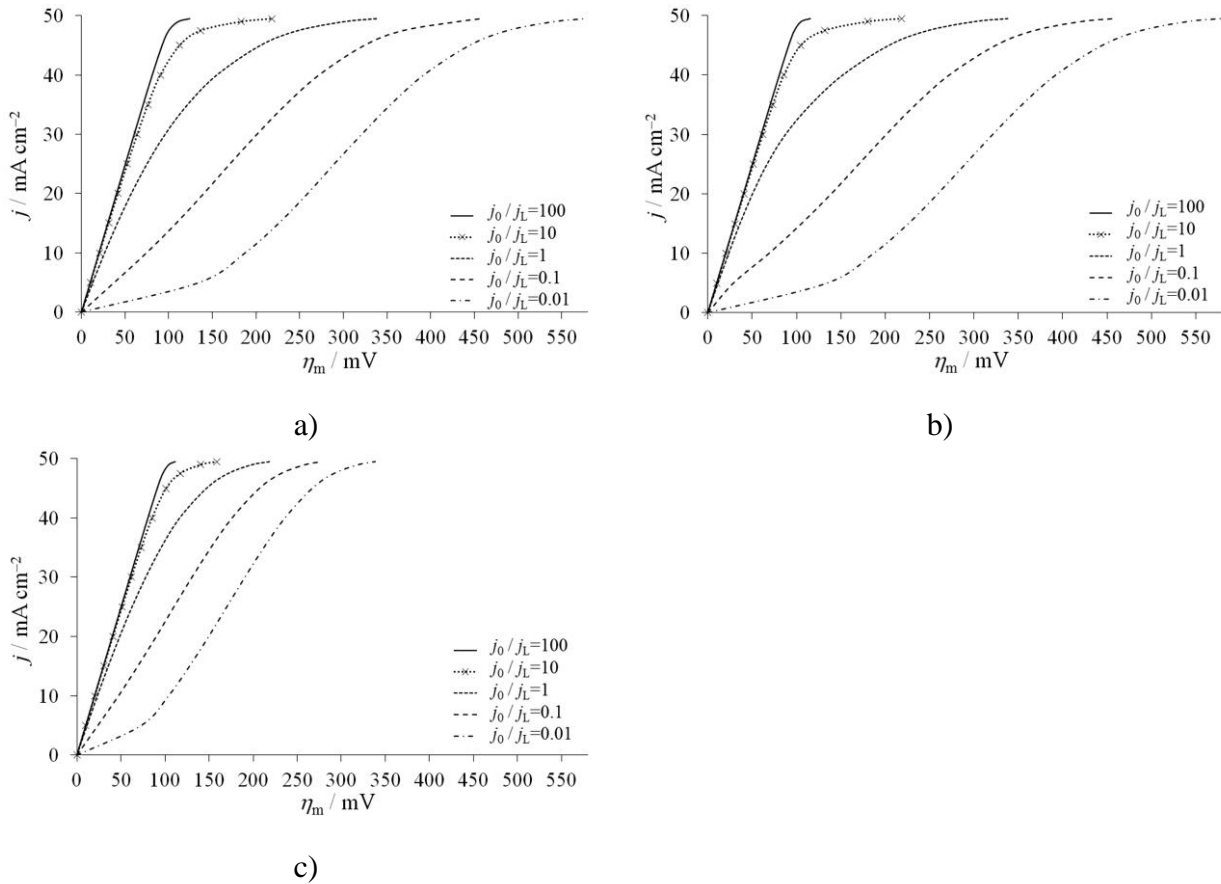
169 Figure 2. Dependencies j - η_m calculated using the Eqs. (2), (3) and (4) and the different values of

170   j_0/j_L ratio for $j_L = 50$ mA cm^{-2}, $L = 0.2$ cm and $\kappa = 0.1$ S cm^{-2}: a), b) and c) as in

171   captions in Fig. 1.

172

173   The polarization curves consist of two parts in the mixed ohmic-diffusion controlled

174 electrodeposition.[12] The first part corresponds the ohmic control (it is the linear part), and the

175 second one corresponds to the diffusion control (Fig. 3). The length of the ohmic part at the

176 polarization curve decreases with decreasing the j_0/j_L ratio values. Assuming that the diffusion

177 control of the electrodeposition process becomes visible at $\eta_m \geq 0.5$ mV, the values of $j_{0.5}/j_L$ at the

178 end of the linear part of polarization curves are calculated and shown in the function of j_0/j_L ratio

179 in Fig. 4 and given in Table 1. It can be seen from Fig. 4 and Table 1 that the linear part of the

180 polarization curve vanishes at $j_0/j_L = 1$. Hence, there is the mixed ohmic – diffusion control in the

181 interval of $1 < j_0/j_L \leq 100$.

a)

b)

c)
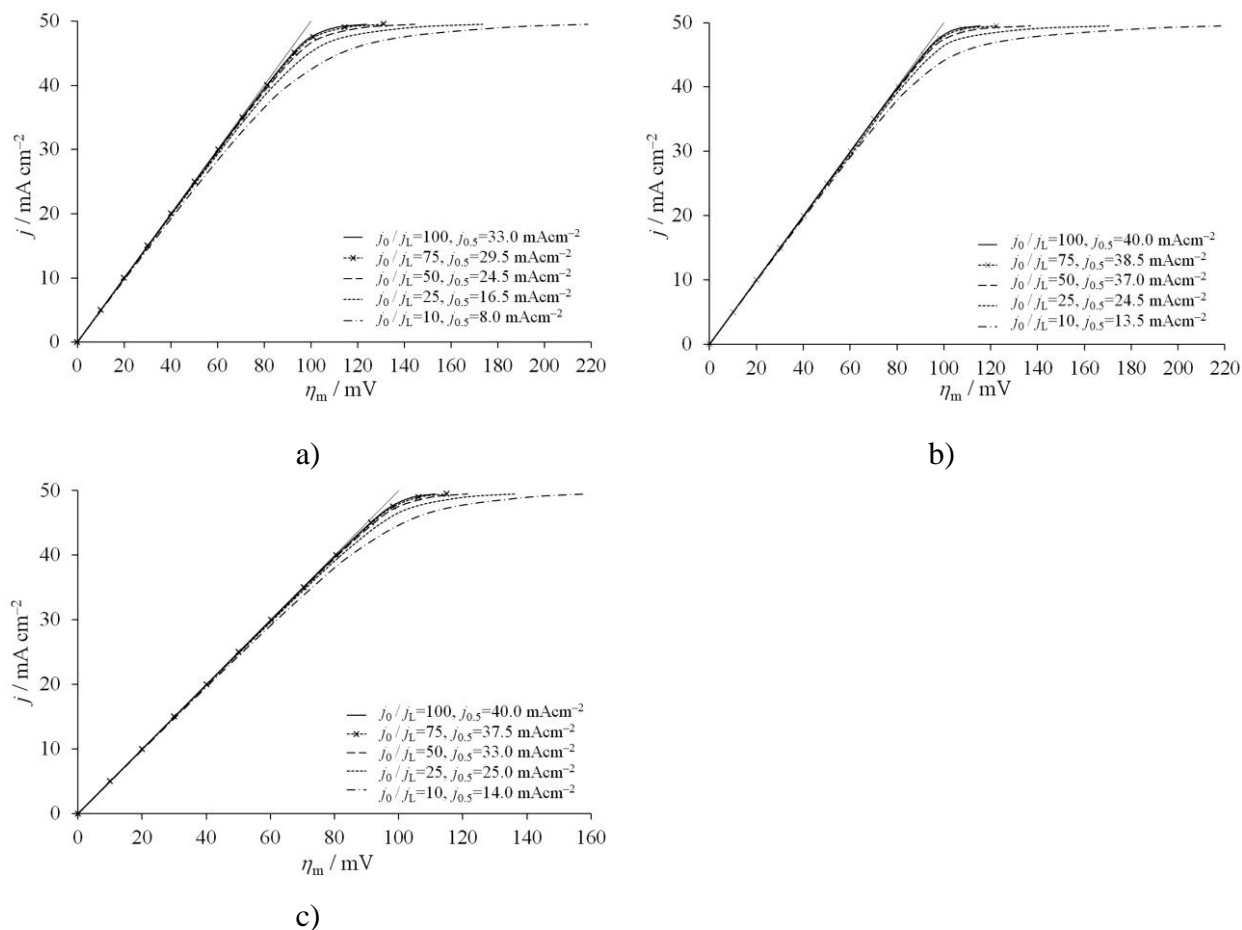
182 Figure 3. Dependencies j - η_m for $10 \leq j_0/j_L \leq 100$ calculated as those in Fig. 2.

183 At values of j_0/j_L ratio lower than 1, the complete diffusion control of the electrodeposition

184 process arises at all overpotentials. The lower limit of the region of the complete diffusion control

185 can be determined as follows: it is obvious that the convex shape of the polarization curve

186 characterizes the diffusion control of deposition process and the concave one the activation

187 control of deposition process. The j/j_L ratio as function of η is shown in Fig. 1 and the j as a

188 function of η_m in Fig. 2. In both cases the convex shape of curves changes in the concave one at

189 approximately $j_0/j_L \sim 0.1$, meaning that the diffusion control changes in the activation one at the

190 beginning of the polarization curve at low η and η_m. At larger overpotentials the diffusion control

191 occurs. Hence, the diffusion control at all overpotentials appears at $0.1 < j_0/j_L \leq 1$, while the

192 activation control appears at $j_0/j_L \leq 0.1$ at low overpotentials.
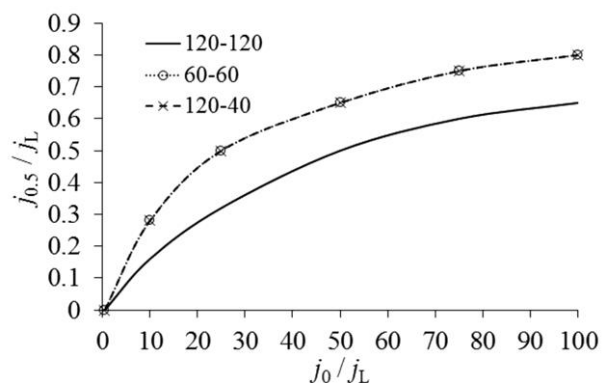
193

194 Figure 4. Dependencies $j_{0.5}/j_L$ ratio on the j_0/j_L ratio. a), b) and c) as in captions in Fig. 1.

195

196 TABLE I. Calculated value of $j_{0.5}$ as function of j_0/j_L ratio. a), b) and c) as in captions in Fig. 1

j_0/j_L	$j_{0.5}$ / mA cm^{-2}		
	a	b	c
10	8.0	13.5	14.0
25	16.5	24.5	25.0
50	24.5	37.0	33.0
75	29.5	38.5	37.5
100	33.0	40.0	40.0

197
198

199 It can be seen from Figs. 1 and 2 that the same conclusion can be derived for the

200 polarization curves with and without included ohmic overpotential drop. The simulated

201 polarization curves with included ohmic drop are calculated using data for 1 M solution of

202 typically fully dissociated electrolyte without supporting electrolyte.[15] It is obvious that for less

203 concentrated solutions with supporting electrolyte (mainly some acid or base) the ohmic potential

204 drop can be neglected. Because of this fact η instead of η_m will be used, except for some special

205 cases indicated.

206

207   *Experimental verification of the simulated polarization curves with the included ohmic potential*

208   *drop*

209

210   The nearest experimental curves to the simulated curves for j_0/j_L =100 (the full ohmic

211   control) and $1 < j_0/j_L \leq 100$ (the mixed ohmic - diffusion control) are recorded during lead

212   electrodeposition processes because electrodeposition of lead occurs in the conditions of the

213   mixed ohmic-diffusion or even full ohmic control.[12] Lead is characterized by the extremely high

214   exchange current density value ($j_0 \rightarrow \infty$; the fast electrochemical processes), and there is no a

215   precise and unique way for the determination of the exchange current density values. For that

216   reason, the comparison of simulated and experimentally recorded polarization curves can be

217   excellent auxiliary method for the aproximative estimation of the exchange current density of

218   lead, as well as the other metals from the group of normal metals. The ratio of the ohmic to the

219   overall control of the electrodeposition increases with increasing concentration of Pb^{2+} so that the

220   electrodeposition process becomes a full ohmic controlled one at high concentrations of Pb^{2+}.[12]

221   The typical Pb polarization curves recorded from solutions of different Pb^{2+}

222   concentrations are shown in Fig. 5. The end of the ohmic control is denoted by vertical solid line,

223   while the inflection point is denoted by vertical dot line. The linear dependence of the current

224   density on the overpotential up to the inflection point corresponds to the full ohmic control, and

225   the current density at the inflection point corresponds to the limiting diffusion current density.[12]

226   As seen from Fig. 5a, the condition of the full ohmic control is fulfilled with concentrations of

227   Pb^{2+} ions of 0.45 M (the linear dependence of j - η up to the inflection point) and furthermore

228   with 0.40 M because the linear dependence of j - η is up to about $j/j_L \approx 0.9$.

229   With decreasing concentration of Pb^{2+} ions (Fig. 5b), electrodeposition of Pb occurs in the

230   conditions of the mixed ohmic-diffusion control. After the inflection point, electrodeposition

231   system remains in the diffusion control and the fast increase in current density with further the

232   increase in overpotential is due to a strong increase of surface area of the electrode caused by

233   instantaneous formation and growth of dendrites. The ratios of j/j_L, where j corresponds to the

234   end of the linear dependence and j_L to the inflection point at the polarization curve were

235   approximate 0.51, 0.46 and 0.46 for 0,20, 0.10 and 0.050 M Pb^{2+}, respectively.

236

237

a)   b)
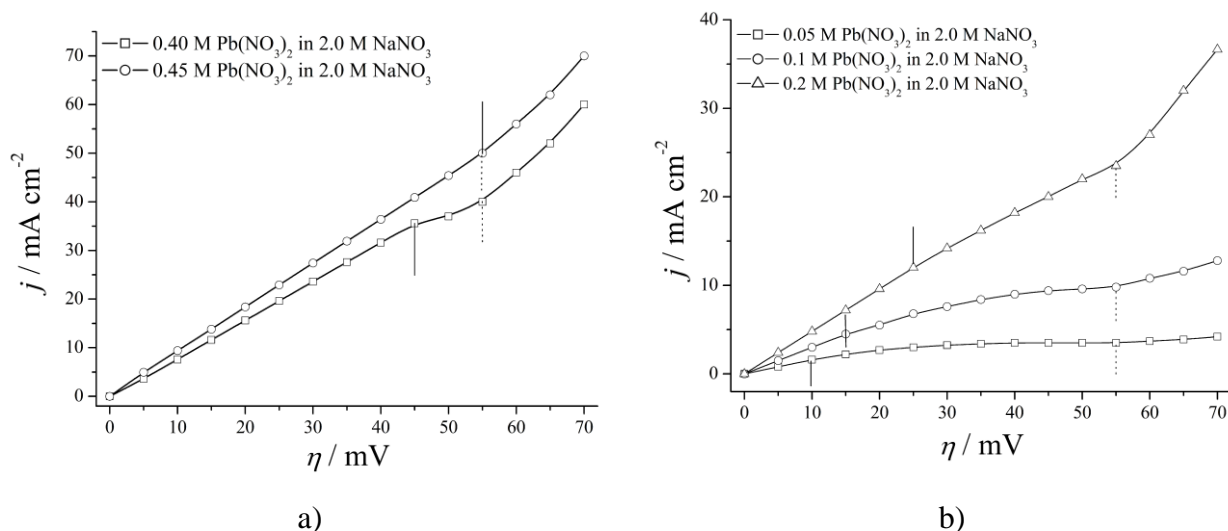
238   Figure 5. The polarization curves for lead electrodeposition from: a) 0.40 and 0.45 M and b)

239   0.050, 0.10 and 0.20 M $Pb(NO_3)_2$ in 2.0 M $NaNO_3$.

240   The typical surface morphologies of lead obtained from 0.10 M $Pb(NO_3)_2$ in 2.0 M

241    $NaNO_3$ are shown in Fig. 6. The regular hexagonal particles are formed by electrodeposition in

242   the ohmic control (Fig. 6a; $\eta = 10$ mV). The elongated irregular particles (precursors of

243   dendrites) and dendrites of the different shape (needle-like and „tooth of saw"-like dendrites)

244   were formed under the diffusion control before (Fig. 6b; $\eta = 50$ mV) and after (Fig. 6c; $\eta = 100$

245   mV) the inflection point at the polarization curve. Following the classical Wranglen definition of

246   a dendrite,[16,17] the dendrites of Pb belong to 2D (two-dimensional) primary (P) type dendrites.

247   The dendrites of lead were very similar to those obtained by silver electrodeposition processes

248   from the nitrate electrolytes,[18-20] indicating on the strong dependence of the shape of dendrites on

249   the affiliation to the determined group of metals.

250

a)   b)   c)
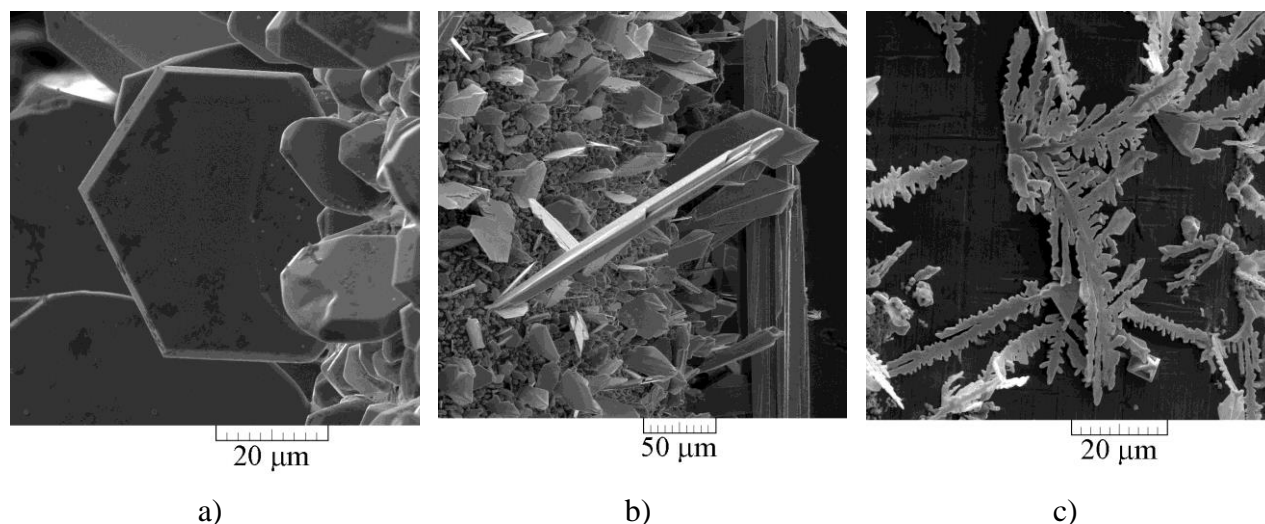
Figure 6. The typical surface morphologies of lead electrodeposited from 0.10 M Pb(NO$_3$)$_2$ in 2.0
M NaNO$_3$ at overpotentials of: a) η = 10 mV (the ohmic control); time of the
electrodeposition (t), t = 25 min, b) η = 50 mV (the diffusion control before the
inflection point), t = 210 s, and c) η = 100 mV (the diffusion control after the inflection
point), t = 140 s.

Zinc also belong to the group of normal metals characterized by $j_0 \rightarrow \infty$, but the shape of
the polarization curve is completely different from those characteristic for Pb. The typical Zn
polarization curve obtained from 0.10 M ZnSO$_4$ in 2.0 M NaOH is shown in Fig. 7a. As seen
from Fig. 7a, there is no the ohmic controlled part at this polarization curve. After the initial part
determined by the low nucleation rate, the shape of polarization curve takes the convex shape up
to a reach of the plateau of the limiting diffusion current density. Comparing this shape of the
polarization curve with the simulated ones, it is clear that Zn is „slower metal" than Pb, with the
ratio $j_0/j_L < 1$.

Morphology of electrodeposited Zn was also completely different from the one observed
during electrodeposition of Pb. Unlike of regular grains formed by Pb electrodeposition, the
spongy particles were formed at overpotentials belonging to the convex shape at the polarization
curve (Fig. 7b; η = 45 mV). Simultaneously, dendrites were electrodeposited at the plateau of the
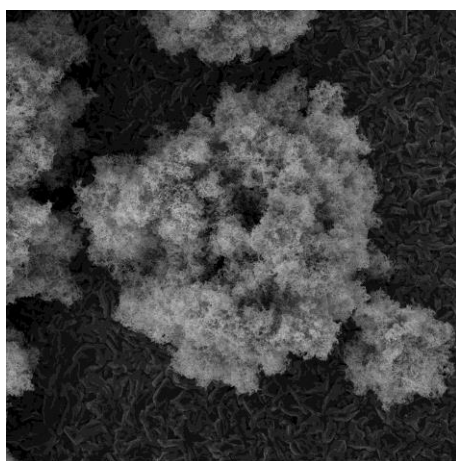limiting diffusion current density (Fig. 7c; η = 100 mV).
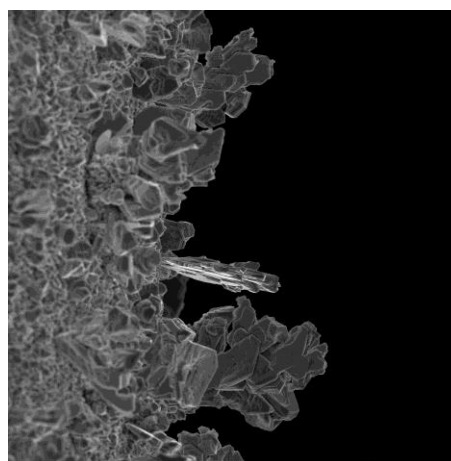
271

a)

20 μm

b)

50 μm
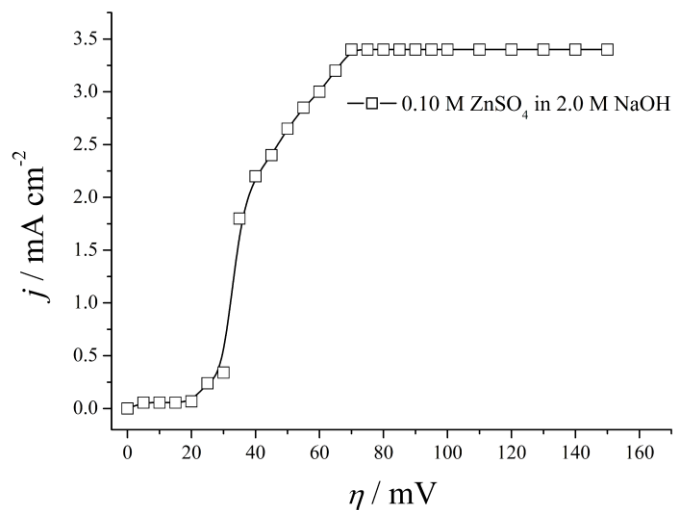
c)

272 Figure 7. a) The polarization curve for Zn electrodeposition from 0.10 M ZnSO₄ in 2.0 M NaOH,

273   and the typical surface morphologies obtained at overpotentials of: b) $\eta = 45$ mV (the

274   zone of the fast increase in the current density with increasing overpotential), $t = 60$ min,

275   and c) $\eta = 100$ mV (the plateau of the limiting diffusion current density), $t = 50$ min.

276   The further lowering the exchange current density leads to the further change of the shape

277 of the polarization curve. As result of this, the initial part of the polarization curve transforms

278 from the convex (the diffusion control) to concave (the activation control) one at approximately

279 $j_0/j_L \leq 0.1$. The typical representative of this group of metals is copper. Namely, Cu belongs to the

280   group of the intermediate metals characterized by the medium exchange current density values.[2,3]

281   The polarization curve obtained from solution containing 0.10 M $CuSO_4$ in 0.50 M H_2SO_4 is

282   shown in Fig. 8a. For this solution,[1] $j_0 = 0.11$ mA cm^{-2} and $j_L = 9.2$ mA cm^{-2} and hence $j_0/j_L =$

283   0.012. This polarization curve consists of four parts: a) activation, b) mixed activation-diffusion,

284   c) diffusion, and d) the zone of the fast increase of current density with overpotential.

285   Electrodeposition in each of these regions produces characteristic surface morphologies. The

286   large grains are obtained in the activation controlled electrodeposition (Fig. 8b). The carrot-like

287   (Fig. 8c) and globular forms (Fig. 8d) are formed in the mixed activation-diffusion control. The

288   3D (three-dimensional) pine-like dendrites formed inside the plateau of the limiting diffusion

289   current density are shown in Fig. 8e. The shape of pine-like Cu dendrites was very similar to Ag

290   dendrites obtained from the various types of complex electrolytes like those with the addition of

291   ammonia[20,21], tungstosilicate[22] and citric[23] acids, or to Au dendrites.[24] In this way, the strong

292   correlation between the surface morphologies and the affiliation to the determined group of

293   metals is confirmed. Due to the lower overpotentials for hydrogen evolution reaction, the effect

294   of evolved hydrogen as parallel reaction to copper electrodeposition at the high overpotentials

295   become visible in the zone of the fast increase of the current density with increasing

296   overpotential. The honeycomb-like structures can be formed in this zone (Fig. 8f).

297   Finally, electrodeposition of metals from the group of inert metals occurs parallel with

298   hydrogen evolution reaction in the whole range of potentials and current densities. The corrected

299   polarization curves can be only obtained after IR drop correction,[25] making their analysis out of

300   scope of this investigation. Due to vigorous hydrogen evolution, the spongy-like and globular

301   particles, as well as degenerate dendrites are formed.[26-28]

302

303   CONCLUSIONS

304

305   The polarization curves for the different the exchange current densities to the limiting

306   diffusion current densities (j_0/j_L) ratios were simulated. The correlation between the shape of

307   polarization curve and the type of metal electrodeposition process control was established on the

308   basis of these ratios. The four diagnostic criteria based on j_0/j_L ratios were established: (a) $j_0/j_L >$

309   100 - the ohmic control, (b) $1 < j_0/j_L \leq 100$ - the mixed ohmic-diffusion control, (c) $0.1 < j_0/j_L \leq 1$

310   - the diffusion control and (d) $j_0/j_L \leq 0.1$ - the activation control at the low overpotentials. The

311 verification of the proposed diagnostic criteria was successfully done by comparison with

312 experimentally obtained polarization curves and by the surface analysis of deposits obtained in

313 the different types of metal electrodeposition process control.

314

315 **Acknowledgement**

316

321

322

323

324

325

326

327
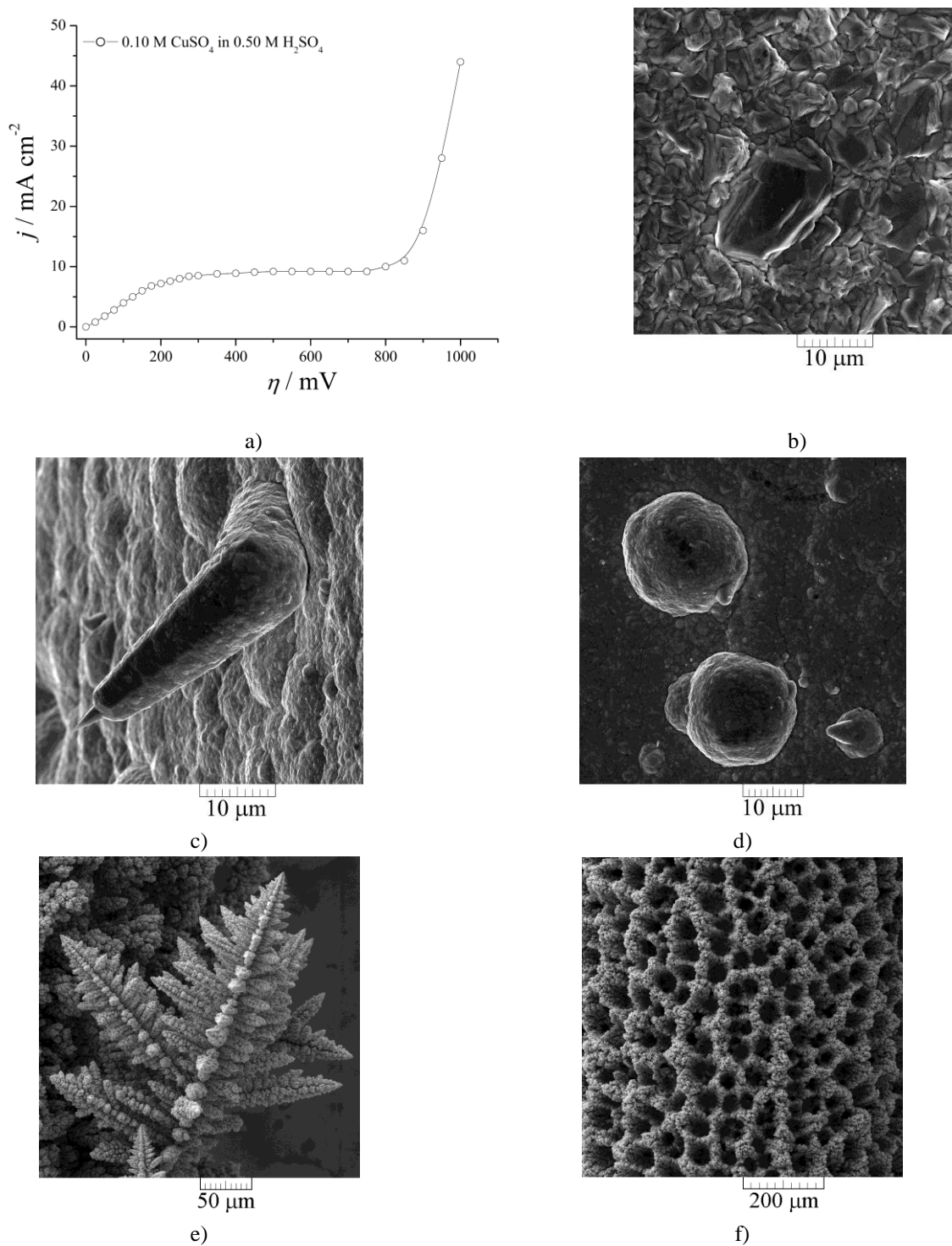
328

329

330

331

332

333

334

335

16

a)

b)

c)

d)

e)

f)

Figure 8. a) The polarization curve for Cu electrodeposition from 0.10 M CuSO$_4$ in 0.50 M H$_2$SO$_4$, and the typical surface morphologies obtained in the different types of control: b) activation, $\eta = 90$ mV; $t = 120$ min, c) and d) activation-diffusion, $\eta = 210$ mV; $t = 45$ min, e) diffusion, $\eta = 650$ mV; $t = 52$ min, and f) zone of the fast increase of current density with overpotential, $\eta = 1000$ mV; $t = 120$ s.

341 <p style="text-align:center">И З В О Д</p>

342

343 <p style="text-align:center">ОБЛИК ПОЛАРИЗАЦИОНЕ КРИВЕ И ДИЈАГНОСТИЧКИ КРИТЕРИЈУМИ ЗА</p>

344 <p style="text-align:center">КОНТРОЛУ ПРОЦЕСА ЕЛЕКТРОХЕМИЈСКОГ ТАЛОЖЕЊА МЕТАЛА</p>

345

346 <p style="text-align:center">КОНСТАНТИН И. ПОПОВ[1,2], ПРЕДРАГ М. ЖИВКОВИЋ[1],</p>

347 <p style="text-align:center">БОЈАН ЈОКИЋ[1] и НЕБОЈША Д. НИКОЛИЋ[2]</p>

348

349 *[1]Технолошко-металуршки факултет, Универзитет у Београду, Карнегијева 4, Београд и*

350 *[2]ИХТМ – Центар за електрохемију, Универзитет у Београду, Његошева 12, Београд,*

351 *Србија*

352

353 Поларизационе криве добијене дигиталном симулацијом су биле корелисане са типом

354 контроле процеса електрохемијског таложења метала у функцији односа густине струје

355 измене и граничне дифузионе густине струје (j_0/j_L). На основу j_0/j_L удела утврђени су

356 дијагностички критеријуми. За $j_0/j_L > 100$, систем је под омском контролом. У опсегу $1 <$

357 $j_0/j_L \leq 100$ постоји мешовита омско-дифузиона контрола. Дифузиона контрола се јавља у

358 опсегу $0.1 < j_0/j_L \leq 1$. За $j_0/j_L \leq 0.1$, систем је активационо контролисан на малим

359 пренапетостима. Предложени дијагностички критеријуми су потврђени поређењем

360 симулираних кривих са експериментално снимљеним кривама и анализом морфологија

361 талога добијених у различитим типовима контроле процеса електрохемијског таложења

362 метала.

363

364

365

366

367

368

369

370

371

372   References

373

374   1. K. I. Popov, S. S. Djokić, B. N. Grgur, *Fundamental aspects of electrometallurgy*, Kluwer

375   Academic/Plenum Publishers, New York, 2002, p.p. 1–305

376   2. R. Winand, *Electrochim. Acta* **39** (1994) 1091

377   3. V. M. Kozlov, L. Peraldo Bicelli, *J. Cryst. Growth* **203** (1999) 255

378   4. K. I. Popov, M. G. Pavlović, Lj. J. Pavlović, M. I. Čekerevac, G. Ž. Remović, *Surf. Coat.*

379   *Technol.* **34** (1988) 355

380   5. A. Damjanović, *Plating* **52** (1965) 1017

381   6. K. I. Popov, B. N. Grgur, M. G. Pavlović, V. Radmilović, *J. Serb. Chem. Soc.* **58** (1993) 1055

382   7. K. I. Popov, V. Radmilović, B. N. Grgur, M. G. Pavlović, *J. Serb. Chem. Soc.* **59** (1994) 47

383   8. K. I. Popov, M. D. Maksimović, J. D. Trnjančev, M. G. Pavlović, *J. Appl. Electrochem.* **11**

384   (1981) 239

385   9. N. D. Nikolić, K. I. Popov, Hydrogen Co-deposition Effects on the Structure of

386   Electrodeposited Copper, in *Electrodeposition: Theory and Practice*, Series: *Modern Aspects*

387   *of Electrochemistry*, S. S. Djokić, Ed., Vol. 48, Springer, 2010, p.p. 1–70

388   10. K. I. Popov, N. V. Krstajić, *J. Appl. Electrochem.* **13** (1983) 775

389   11. K. I. Popov, P. M. Živković, N. D. Nikolić, The Effect of Morphology of Activated

390   Electrodes on their Electrochemical Activity, in *Electrodeposition: Theory and Practice*,

391   Series: *Modern Aspects of Electrochemistry*, S. S. Djokić, Ed., Vol. 48, Springer, 2010, p.p.

392   163–213

393   12. N. D. Nikolić, K. I. Popov, P. M. Živković, G. Branković, *J. Electroanal. Chem.* **691** (2013)

394   66

395   13. N. D. Nikolić, V. M. Maksimović, G. Branković, P. M. Živković, M. G. Pavlović, *J. Serb.*

396   *Chem. Soc.* **78** (2013) 1387

397   14. N. D. Nikolić, K. I. Popov, E. R. Ivanović, G. Branković, *J. Serb. Chem. Soc.* **79** (2014) 993

398   15. J. O' M. Bockris, A. K. N. Reddy, M. Gamboa-Aldeco, *Modern Electrochemistry 2 A*, 2nd

399   edition, Kluwer/Plenum, New York, 2000, p. 1107

400   16. G. Wranglen, *Electrochim. Acta* **2** (1960) 130

401   17. H. M. Liaw, J. W. Faust Jr, *J. Cryst. Growth* **18** (1973) 250

402   18. C. Ding, C. Tian, R. Krupke, J. Fang, *CrystEngComm* **14** (2012) 875

403   19. R. Sivasubramanian, M. V. Sangaranarayanan, *CrystEngComm* **15** (2013) 2052

404   20. S. S. Djokić, N. D. Nikolić, P. M. Živković, K. I. Popov, N. S. Djokić, *ECS Trans.* **33** (2011)
405   7

406   21. N. D. Nikolić, P. M. Živković, B. Jokić, M. G. Pavlović, J. S. Stevanović, *Maced. J. Chem.*
407   *Chem. Eng.* **33** (2014) 169

408   22. J. Han, J. Liu, *J. Nanoeng. Nanomanuf.* **2** (2012) 171

409   23. M. V. Mandke, S-H. Han, H. M. Pathan, *CrystEngComm* **14** (2012) 86

410   24. Z- Y. Lv, A- Q. Li, Y. Fei, Z. Li, J- R. Chen, A- J. Wang, J- J. Feng, *Electrochim. Acta* **109**
411   (2013) 136

412   25. V. D. Jović, B. M. Jović, M. G. Pavlović, *Electrochim. Acta* 51 (2006) 5468

413   26. L. Vazquez-Gymez, E. Verlato, S. Cattarin, N. Comisso, P. Guerriero, M. Musiani,
414   *Electrochim. Acta* 56 (2011) 2237

415   27. J. Wang, L. Wei, L. Zhang, Y. Zhang, C. Jiang, *CrystEngComm* **14** (2012) 1629

416   28. V. M. Maksimović, N. D. Nikolić, V. B. Kusigerski, J. L. Blanuša, *J. Serb. Chem. Soc.* **80**
417   (2015) 197.